




Cancer vaccine designed from homologous ferritin-based fusion protein with enhanced DC-T cell crosstalk for durable adaptive immunity against tumors

Jun Wu^{a,b}, Jing Liang^a, Sichen Li^a, Jinjin Lu^a, Yi Li^a, Bin Zhang^a, Min Gao^a, Juan Zhou^a, Yan Zhang^{a,**}, Jinghua Chen^{a,*} 

^a School of Life Sciences and Health Engineering, Jiangnan University, Wuxi, 214122, PR China

^b School of Chemical & Material Engineering, Jiangnan University, Wuxi, 214122, PR China

ARTICLE INFO

Keywords:

Peptide vaccine
Nanovaccine
Ferritin
siRNA delivery
Cancer immunotherapy

ABSTRACT

Peptide vaccines based on tumor antigens face the challenges of rapid clearance of peptides, low immunogenicity, and immune suppressive tumor microenvironment. However, the traditional solution mainly uses exogenous substances as adjuvants or carriers to enhance innate immune responses, but excessive inflammation can damage adaptive immunity. In the current study, we propose a straightforward novel nanovaccine strategy by employing homologous human ferritin light chain for minimized innate immunity and dendritic cell (DC) targeting, the cationic KALA peptide for enhanced cellular uptake, and suppressor of cytokine signaling 1 (SOCS1) siRNA for modulating DC activity. Upon fusing with the KALA peptide, this nanovaccine presents as a novel 40-mer cage structure, with highly enriched antigen peptides of proper size (25 nm) for targeted delivery to lymph nodes. The loading of SOCS1 siRNA onto the KALA peptide promoted DC maturation in tumor environment, leading to a 3-fold increase in antigen presentation compared to alum adjuvant. Moreover, it demonstrates remarkable efficacy in suppressing tumor progression and metastasis, together with prolonged survival. In addition, the nanovaccine stimulates up to 40 % memory T cells, thereby achieving sustained protection against tumor re-challenge. This unprecedented nanovaccine platform can ignite fresh interdisciplinary discussions on interactive strategies for future peptide vaccine development.

1. Introduction

Cancer immunotherapy has been acclaimed as a revolutionary breakthrough in tumor treatment [1–3]. Differing from other immunotherapies, cancer vaccines harness innate immunity—rapid, transient non-specific inflammation and phagocytosis—to initiate adaptive immunity. This process induces specific cytotoxic responses and generates memory cells for long-term protection [4–7]. Peptide vaccines, integrated with specific or associated antigenic epitopes to guide T-cell immune responses [5–7], have demonstrated favorable biosafety, tolerability, and low production costs, leading to a higher number of clinical trials compared to other types of cancer vaccines [8]. However, a review of clinical data on peptide vaccines from 1995 to 2004, involving approximately 323 patients, revealed a mere 2.9 % objective response rate [9,10]. These unsatisfactory immune responses can be attributed to

the low stability of peptides that are susceptible to *in vivo* degradation, ineffective antigen transport to draining lymph nodes, as well as the low immunogenicity caused by tumor antigens derived from patient themselves and immune-suppressive environments [11–13].

To address these challenges, numerous of exogenous materials, including lipids, synthetic copolymers and protein nanocages derived from bacteria or viruses, have been engineered for antigen protection and targeted delivery to lymph nodes [10,12–14]. Additionally, to boost immunogenicity further, researchers have incorporated adjuvants like aluminum salts [15,16], emulsions [17,18], and specific pattern recognition receptor (PRR) ligands into the formulations [19–21]. However, the combined use of different adjuvants is frequently required to trigger simultaneous immune stimulation through diverse mechanisms for sufficient responses [22]. With deeper exploration of immuno-oncology, exogenous stimuli-induced inflammation was found critical in

* Corresponding author.

** Corresponding author.

E-mail addresses: zhangyanyanz@jiangnan.edu.cn (Y. Zhang), chenjinghua@jiangnan.edu.cn (J. Chen).

<https://doi.org/10.1016/j.bioactmat.2024.12.029>

Received 5 July 2024; Received in revised form 30 September 2024; Accepted 27 December 2024

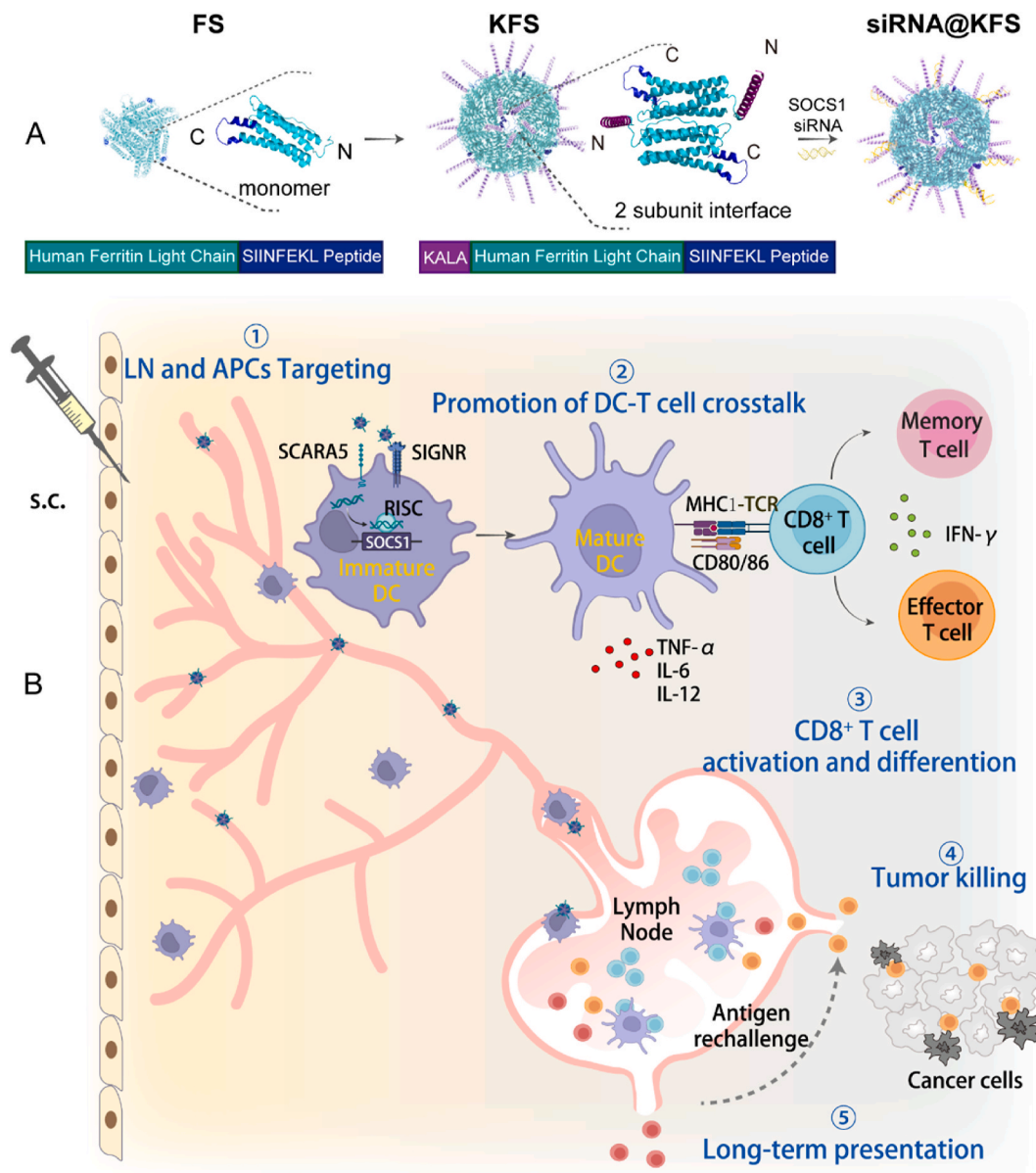
2452-199X/© 2024 The Authors. Publishing services by Elsevier B.V. on behalf of KeAi Communications Co. Ltd. This is an open access article under the CC BY-NC-ND license (<http://creativecommons.org/licenses/by-nc-nd/4.0/>).

weakening the adaptive immunity. For example, *Listeria monocytogenes*, used as a cancer vaccine carrier due to its selective infection of host antigen presenting cells (APCs) and activation of NAIP-NLRC4 inflammasome, can dampen memory CD8⁺ T cell responses from excessive inflammation [23,24]. *Helicobacter pylori*, as a TLR5 agonist, promotes the production of IL-18 and TNF- α , activating the innate immunity while also aggravating the activity of Treg cells, thereby causing immune evasion [25,26]. Over-activation of the innate immune system leads to adverse effects and disrupts the balance between innate and adaptive immunity, potentially compromising vaccine efficacy.

Dendritic cells (DCs), as a frontline warrior in initiating anti-tumor immune responses, however, mostly remain in an immature state within the immune suppressive microenvironment of tumors, resulting

in inadequate antigen capture, presentation, and T cell recruitment and activation [27]. In this regard, STAT3, SOCS, and BACH play key roles in modulating the activation and differentiation processes in APCs and T cells [28,29]. Among these, suppressor of cytokine signaling 1 (SOCS1), overexpressed in functionally defective immature DCs within the tumor microenvironment [30], functions as a negative feedback regulator. It mediates the inhibition of Janus kinases (JAKs) and the IFN-I signaling pathway, thereby impacting DC-T cell crosstalk and T cell proliferation [31–33]. For example, SOCS1 has been utilized in engineered DC vaccines for the treatment of relapsed acute leukemia, resulting in an impressive 83 % complete remission rate in the clinical trial (NCT01956630) [34].

Considering the challenges faced by peptide vaccines, including



Scheme 1. Schematic illustration of the ferritin-based nanovaccine for co-delivery of antigens and SOCS1 siRNA in cancer therapy and prevention. A) Preparation of the ferritin-based nanovaccines by fusing a T cell antigen epitope at the C-terminus of ferritin light chain (FS), and an additional cationic peptide KALA at the N-terminus (KFS), with subsequent loading of siRNA (siRNA@KFS) through electrostatic interactions. B) The nanovaccine initiates anti-tumor immune responses. 1. Upon subcutaneous injection, its suitable size facilitates rapid migration into lymph nodes, where the enhanced affinity for APCs from ferritin light chain simultaneously promotes targeting effect. 2. Co-delivered SOCS1 siRNA effectively enhance the crosstalk between DCs and T cells, thus improving antigen presentation, co-stimulatory factors and cytokine expression. 3. The nanovaccine induces adaptive immunity, mature DCs efficiently present antigens to CD8⁺ T cells, promoting their activation and subsequent transformation into cytotoxic effector T cells and memory T cells. 4. Effector T cells infiltrate the tumor site to kill tumor cells. 5. The abundance of memory T cells provide long-term immune protection, preventing cancer recurrence.

rapid clearance, low immunogenicity, and immune suppression, we utilized a fusion protein as the nanovaccine, employing human ferritin for antigen stability and DC-targeting, KALA peptide (WEAK-LAKALAKALAKHLAKALAKALKA) for siRNA delivery and cell-penetrating capacities, and SOCS1 siRNA for immune modulation. Human ferritin light chain was used here to fuse interchangeable tumor antigens, for its high stability and enriched antigen display abilities [35] (Scheme 1). Different from the commonly used ferritin derived from *Helicobacter pylori*, which poses potential risks to adaptive immunity [36–40], human ferritin is highly homologous that can minimize adverse effects associated with over-activated innate immunity. In addition, the ferritin light chain has been demonstrated extra affinity for DC surface receptors SCARA5 and SIGNR compared to the heavy chain, thereby enhancing the chances of antigen uptake by APCs [41,42]. Furthermore, SOCS1 siRNA was co-loaded to activate the JAK/STAT pathway through the binding with KALA peptide, thus addressing the low immunogenicity of homologous ferritin and promoting DC maturation in the tumor environment. This all-in-one multifunctional nanovaccine offers a novel strategy to enhance DC-T cell crosstalk without introducing exogenous stimuli, thereby maintaining the smooth cycle of innate-adaptive tumor immunity, and achieving efficient and long-lasting anti-tumor immune protection.

2. Results

2.1. Constructing nanovaccines for simultaneous delivery of antigen and siRNA

In this study, we engineered the human ferritin light chain (L-ferritin) to incorporate the SIINFEKL epitope and the KALA peptide on the C- and N-terminal sequences, respectively [43]. Structural simulations of monomeric and dimeric states of the fusion protein (Figs. S1–2) confirmed its optimal antigen presentation and RNA-binding

capabilities (Fig. 1A) [44,45]. Thereafter, this dual-functional fusion protein (KFS), along with the original human ferritin light chain (F), the C-SIINFEKL terminated ferritin (FS), and the N-KALA terminated ferritin (KF), were expressed in *E. coli* and purified using affinity chromatography (Fig. S3). The exact molecular weights of the protein subunits were measured by LC-MS, and the results aligned with their theoretical calculations (Figs. S4–S7). The incorporation of the KALA peptide was confirmed by the positively charged protein surfaces of the obtained ferritin-based fusion proteins (Fig. 1B), with 80.7 and 62.3 mV for KFS and KF, respectively, as compared to -5.96 mV for ferritin alone (F). Moreover, the introduction of the KALA peptide (KF and KFS) resulted in significant changes in the aggregation status of ferritin, as demonstrated by both dynamic light scattering (DLS) and size exclusion chromatography (SEC) analyses (Fig. 1C & Fig. S8), with the particle sizes increased from 12 nm for FS to approximately 25 nm for KF and KFS. This specific particle size is well-suited for traversing the matrix and entering the initial lymphatic vessels through cell junctions, while avoiding accelerated clearance effects caused by excessively small sizes (<10 nm) [46]. The polymeric states of the fusion protein were further determined through SEC-HPLC and native PAGE analysis, resulting in altered assembly pattern of the proteins upon the introduction of KALA peptide, as supported by the molecular weights of forty-mer structures for KFS and KF in Fig. 1D and Figs. S9–11. Additionally, circular dichroism measurements on the ferritin-based fusion proteins also confirmed the substantial alterations in secondary structures upon the introduction of the KALA peptide (Fig. S12). The significantly increased aggregation of the KFS protein can be attributed to the positively charged residues of the KALA peptide at the N-terminus, along with the enhanced hydrophobic interactions. This results in the formation of protein nanocages of a more polymorphous state, increasing the density of antigens and siRNA binding sites for further immunotherapy applications [47,48].

In addition to the fused antigen in the proteins, SOCS1, as an

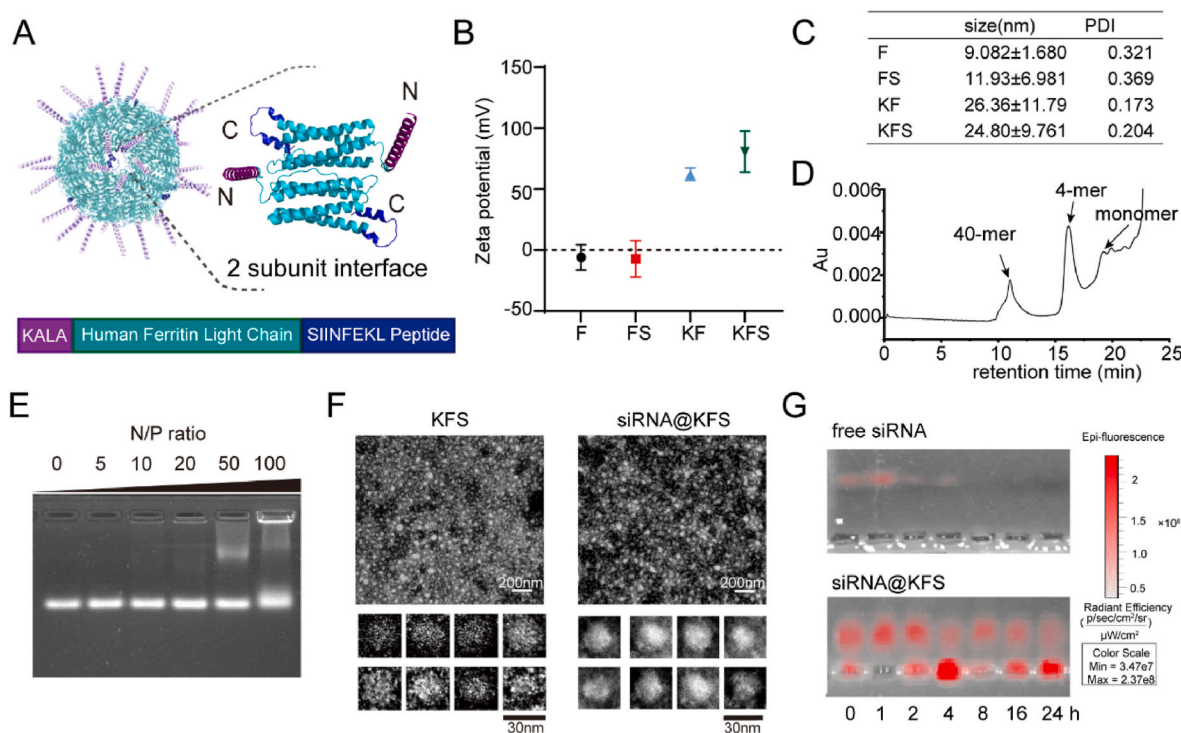


Fig. 1. Design and characterization of the nanovaccines.

(A) Schematic illustration of the fused protein KFS. The NH₂- and COOH- termini are labelled as N and C, respectively. (B) Zeta potentials of different recombinant ferritin-based vaccines. (C) Size of different recombinant ferritin-based vaccines. (D) HPLC-SEC of KFS. (E) Agarose gel retardation assay of binding affinity of KFS/siRNA complexes with different N/P ratios. (F) Transmission electron microscopy images of KFS, and KFS loaded with siRNA at N/P ratio of 50. (G) Stability of the KFS loaded siRNA in 50% serum at 37 °C.

inhibitory regulatory gene in antigen-presenting cells, was selected as the co-delivered siRNA to control the dendritic cell antigen presentation and adaptive immune response intensity [30,31]. Initially, the siRNA payloads of **KFS** were assessed by incubating the protein with siRNA at different N/P molar ratios. As a result, gel electrophoresis showed slower migrating bands of the **KFS** presenting group with the increase of N/P ratio (Fig. 1E). Meanwhile, the surface Zeta potential of **KFS** gradually decreased with the added amount of siRNA (Fig. S13), from positive 80.7 mV of **KFS** alone to 0 mV when N/P equals 10, demonstrating the binding and charge neutralization process. The transmission electron microscopy (TEM) (Fig. 1F) also revealed slightly larger sizes of the **KFS** nanoparticles after loading of siRNA, with the observation of filamentous siRNA material and a less distinct outline of the protein surfaces. Moreover, the protein-siRNA complex showed excellent resistance to degradation in serum (Fig. 1G), remaining undegraded even after 24 h, while free siRNA was completely degraded within 8 h. Additionally, the nanovaccine demonstrates strong resistance to nucleases (Fig. S14). The stability of **KFS** was further evaluated by measuring its particle size, polydispersity index (PDI), and Zeta potential in saline at 4 °C over a week. As a result, no significant changes in these parameters were observed over the 7-day period, indicating good stability of **KFS** under these conditions (Fig. S15.) This remarkable stability paves the way for downstream *in vitro* and *in vivo* applications.

2.2. Targeting effect for lymph nodes and antigen-presenting cells

Ferritin has been reported to have inherent affinity for SIGNR1-positive APCs, with a higher binding ability to SCARA-5 receptors by the light chain. This feature can guide the system for targeted delivery to APCs, including conventional dendritic cells (cDC) and marginal zone macrophages in draining lymph nodes [38]. Therefore, the *in vivo* distribution of nano-proteins was tracked at different time points in mice. After subcutaneous injection of equimolar amounts of Cy5-modified SIINFEKL antigenic peptide and **KFS** at the tail base, the **KFS** nanovaccine exhibited greater accumulation in lymph nodes at 8 h compared to the antigenic peptide (Fig. 2B), and this effect still maintained at 12 h (Fig. S17).

Given the challenges of cellular uptake of proteins and nucleic acids due to their hydrophilicity, negatively charged surface, and large molecular weight, the KALA segment was delicately incorporated into **KFS** to facilitate the uptake process, while the ferritin structure was engineered for specific recognition by APCs. After verifying the non-toxicity of the nanovaccine in APCs (Fig. S18), the protein or the siRNA was individually fluorescently-labelled for internalization studies of the vaccine levels in the APCs. The results show that **KFS**, even when loaded with siRNA, maintained its high degree of internalization compared to **FS** and free antigenic peptides, with respect to both quantity and rate (Fig. 2C–D and Figs. S19–20). Using HEK293 cells with minimal endogenous receptor expression on the surface as a control, a significantly greater amount of **KFS** particle internalization in DCs was observed after 30 min of incubation and washing, while virtually no particles were detected on the membrane of HEK293 cells (Fig. 2E). Therefore, the rapid cellular uptake of **KFS** can be attributed to the specific affinity between ferritin and the immature DC surface receptor SIGNR and SCARA-5 [38]. Subsequently, the intracellular trafficking of the particles was investigated to achieve functional siRNA delivery in the cytoplasm. As shown in Fig. 2F and Fig. S21, the co-localization of nanoparticles and lysosomes or endosomes was diminished after 4 h of incubation, allowing siRNA to effectively escape from the endosomes. This capability makes **KFS** a viable option for siRNA delivery. Therefore, **KFS**, as a co-delivery platform for antigen and siRNA, provides more opportunities for immune cell interaction and activation, leading to more robust and powerful immune responses.

2.3. *In vitro* DC-T cell crosstalk promotion and T cell activation

DC maturation is essential for initiating immune responses to antigen presentation, while silencing of negative immune-regulatory molecules expressed on dendritic cells through RNA interference can provide a strategy to enhance the efficacy of DC-based immunotherapy. Therefore, quantitative PCR was employed to test the silencing efficiency of the SOCS1 siRNA-loaded fusion protein in immature mouse bone marrow-derived dendritic cells (BMDCs) after 24 h transfection. Compared to untreated cells and the free siRNA group, **KFS** nanoparticles loaded with SOCS1 siRNA (**siRNA@KFS**) achieved an approximate 70 % silencing efficiency at a carrier/nucleic acid N/P ratio of 50. Subsequently, the transcription levels of the JAK/STAT pathway mediated by SOCS1 in different groups were also measured. As the expression levels of the *Socs1* gene decreased, the levels of *Jak1* and *Stat1* genes showed a significant increase, suggesting successful transfection and functionalization of the siRNA (Fig. 3A). The protein expression levels of the three genes were subsequently analyzed using Western Blot, which showed a trend consistent with the qPCR data (Fig. 3B). The maturation level of DCs was then evaluated based on cytokine secretion and cell surface markers. As a result, the levels of inflammatory cytokines IL-6 and TNF- α were significantly elevated, surpassing those of the free antigenic peptide and the physical mixture of antigenic peptide and free SOCS1 siRNA. Additionally, the nanovaccine also successfully activated DCs to express higher levels of IL-12, which is known to promote Th1 cell differentiation, enhance cellular immune responses, and facilitate immune memory (Fig. 3C) [49]. Furthermore, a substantial expression of co-stimulatory molecules CD80/86 was observed (Fig. 3D), indicating a higher degree of DC maturation in the ferritin-based vaccine with enriched antigenic peptides than the free antigenic peptide. Antigen presentation capability of BMDCs after different vaccine treatments were subsequently analyzed. As can be seen in Fig. 3E, there was an increased presentation of MHC-I-SIINFEKL on the surface of BMDCs was observed, suggesting enhanced surface antigen presentation following DC maturation. To ascertain whether DCs were specifically stimulated by the vaccine to promote T cell activation, T cell proliferation and cytokine release in co-cultures of T cells and DCs were examined (Fig. 3F). Initially, mouse splenic T cells (CD3⁺T cells) were isolated and stained with carboxyfluorescein succinimidyl amino ester (CFSE), which were further put into co-culture with DCs at a ratio of 5:1. Flow cytometry measurements revealed a significantly decreased population of CFSE-stained cells in the **siRNA@KFS** group, indicating a higher frequency of T cell division (Fig. 3G–H). Furthermore, the supernatant from the co-cultivation was collected to further measure the cytokines expression. ELISA analysis showed higher levels of IL-6, TNF- α , and IFN- γ secretion after the stimulation of **siRNA@KFS** or **KFS** (Fig. 3I–K), indicating increased T cell activity due to the enhanced functions of DCs.

2.4. The nanovaccine demonstrates a robust immune response *in vivo*

To examine the *in vivo* multifunctionality of the nanovaccine loaded with SOCS1 siRNA, its ability to silence the immune-suppressive environment was examined, along with the promotion effects for DCs maturation and subsequent antigen presentation, and further stimulation of T-cell immune responses. The FDA-approved aluminum adjuvant was also employed as an additional control to evaluate immune effects of the nanovaccine alone without the presence of adjuvants. On a B16-OVA melanoma model, the tumor-draining lymph nodes of the mice were harvested after 7 days of immunization. The expression levels of SOCS1 protein within the lymph nodes were examined using immunohistochemistry (IHC), resulting in a significant reduction in SOCS1 expression by the nanovaccines (Fig. 4B). Meanwhile, flow cytometric analysis of the harvested spleens of mice revealed the highest levels of CD80⁺/86⁺ in DCs after vaccination with **siRNA@KFS** (Fig. 4C and D). Notably, mice immunized with **siRNA@KFS** also exhibited the highest levels of SIINFEKL-H2kb⁺ in CD11c⁺ cells (Fig. 4E). These findings

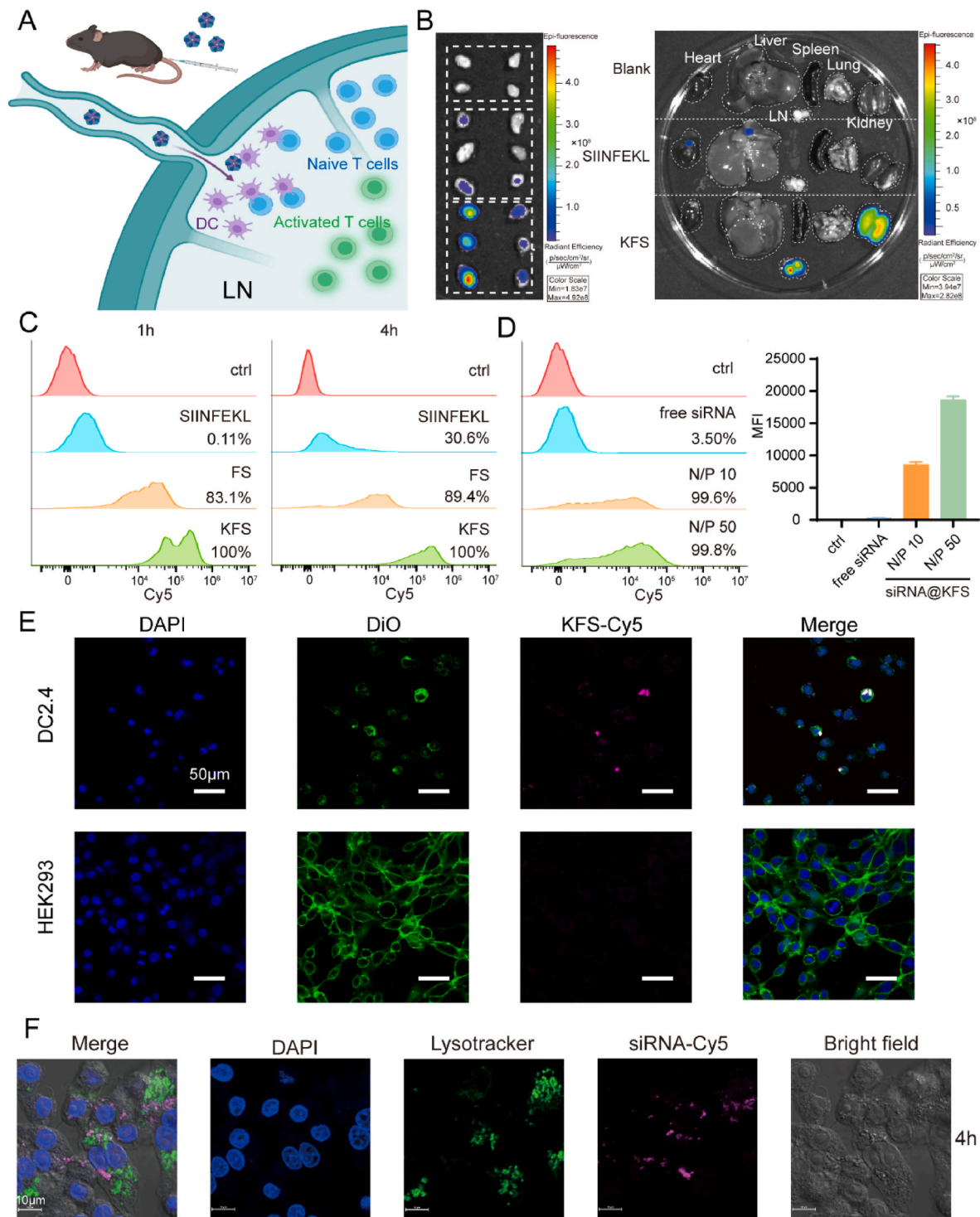
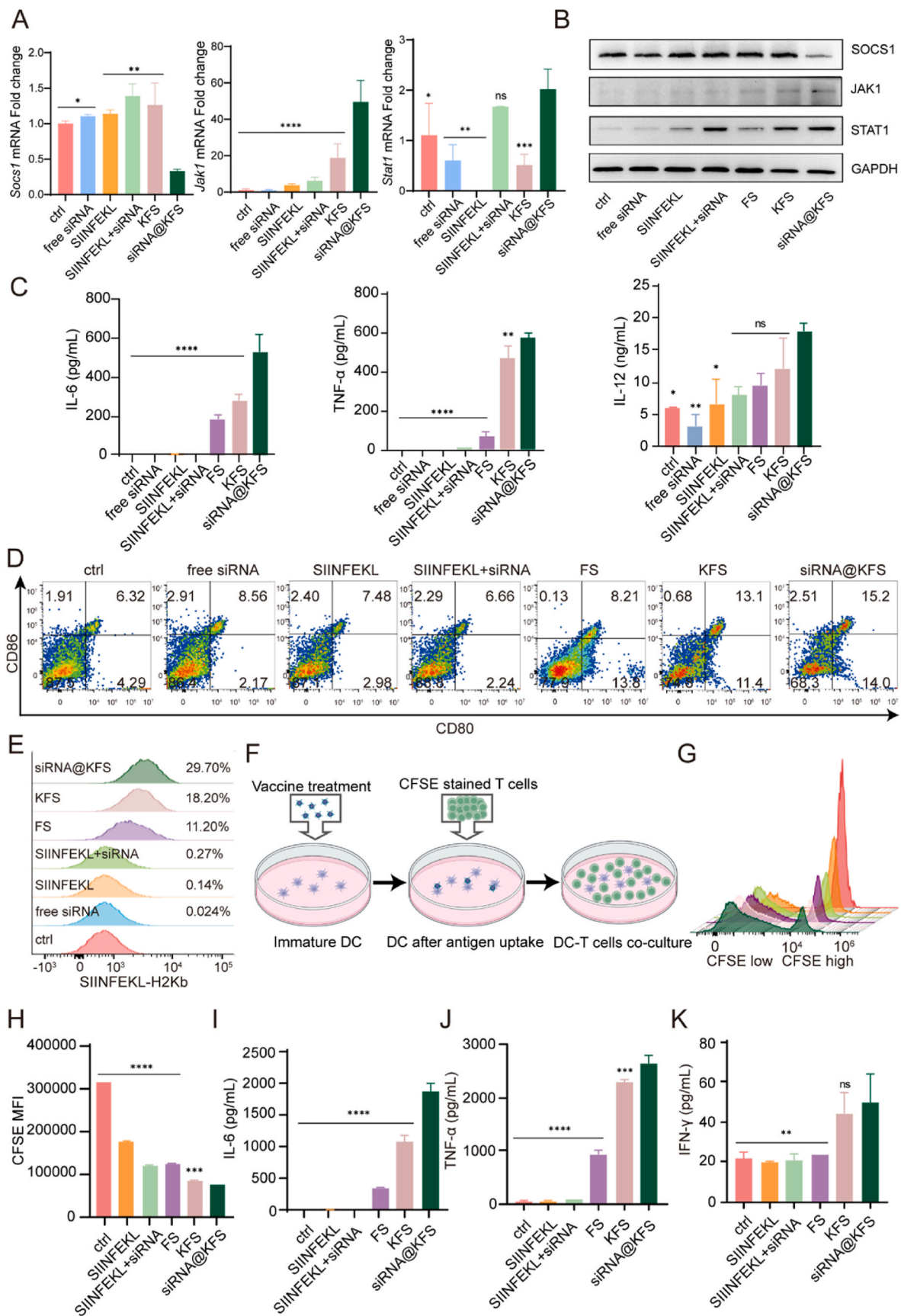


Fig. 2. Targeting effect and cellular uptakes of the nanovaccines. (A) Schematic illustration of the subcutaneous injection of the fusion protein KFS to target lymph nodes at the tail base of a mouse. (B) *Ex vivo* fluorescent imaging of the major organs and inguinal lymph nodes. Cy5-modified KFS or Cy5-modified free antigen peptide SIINFEKL was subcutaneously injected into mice at the tail base. Inguinal lymph nodes and major organs were harvested at 8 h post injection and examined by *in vivo* imaging system (IVIS). (C) Cellular uptake of different Cy5-modified vaccines in bone marrow-derived dendritic cells (BMDCs) at 1 h and 4 h. (D) Cellular uptake of free siRNA-Cy5 or siRNA-Cy5-loaded KFS at N/P ratio 10/50 in BMDCs for 4 h, determined by flow cytometry. (E) DC2.4 and HEK293 cells incubated with Cy5-labelled KFS at 37 °C for 30 min. Cell binding was assessed by confocal laser scanning microscope (CLSM). Green fluorescence, cell membrane stained with DiO; Blue fluorescence, nucleus stained with DAPI. Scale bar, 50 μ m. (F) CLSM images of RAW 264.7 cells treated with siRNA-loaded KFS for 4 h. Magenta fluorescence, siRNA-Cy5; Green fluorescence, endosome/lysosome stained with LysoTracker Green; Blue fluorescence, nucleus stained with DAPI. The red fluorescence shows siRNA escape from endosomal sequestration. Scale bar, 10 μ m.



(caption on next page)

Fig. 3. Nanovaccines promote DC maturation and antigen presentation, activating T cells *in vitro*. (A) The relative gene expression levels of *Socs1*, *Jak1*, and *Stat1* in immature DCs treated with **KFS** loaded with anti-SOCS1 siRNA (**siRNA@KFS**) and other comparison groups, including free siRNA, SIINFEKL peptide, a physical mixture of SIINFEKL peptide and equimolar siRNA, and **KFS**. (B) The protein expression of SOCS1, JAK1 and STAT1 in cell lysates of BMDCs were analyzed by Western blot after treatment with different groups for 48 h. (C) ELISA analysis of IL-6, TNF- α and IL-12 concentrations in supernatants of BMDC culture after a 24 h incubation with PBS, free siRNA, SIINFEKL peptide, physical mixture of SIINFEKL peptide and equimolar siRNA, **FS**, **KFS** and siRNA-loaded **KFS** as **siRNA@KFS**. (D) Expression of CD80 and CD86 in BMDC after treatment with the same formulations as panels. (E) Quantification of OVA-positive BMDC after treatment with the same formulations as panels. (F) Schematic illustration of the experiment on T cell proliferation and the release of cytokines. (G–H) Mean fluorescence intensity distribution of CFSE-stained T cells, incubated with BMDCs that treated with different vaccines. (I–K) Cytokines release from T cells induced by incubation with BMDCs that treated with different vaccines. Representative data are shown and expressed as the mean \pm s.d. Statistical significance was estimated by one-way ANOVA: * $p < 0.05$, ** $p < 0.01$, *** $p < 0.001$, **** $p < 0.0001$. ns, not significant.

signified the successful improvement of the nanovaccine in alleviating the immunosuppressive conditions of DCs within the tumor microenvironment, leading to DC maturation and enhanced antigen-presenting capabilities.

CD8⁺ T cells play a crucial role in cancer immunotherapy. However, prolonged exposure to persistent antigens or inflammatory signals leads to T cell exhaustion, resulting in the gradual deterioration of CD8⁺ cell function, accompanied by the expression of multiple inhibitory receptors, reduced memory capacity, and slowed proliferation within the body [50]. Therefore, the quantity of CD8⁺ cells *in vivo* and the expression of relevant cytokines were further examined. The number of CD8⁺ cells in the spleen also increased compared to other groups (Fig. 4F). The decreased number of CD8⁺ cells in the antigen peptide mixed aluminum adjuvant group can be attributed to the CD8⁺ cell exhaustion that caused by strong inflammatory responses [51]. Moreover, the IFN- γ levels in mouse serum on days 7, 14, and 21 after vaccine injection were assessed to evaluate T cell long-term memory levels (Fig. 4G). On the 7th day, significantly higher IFN- γ level was observed for the **siRNA@KFS** group, even more than three times higher than that of free antigenic peptide or combined with aluminum adjuvant groups. Thereafter, the nanovaccine group maintained elevated levels of interferon for an extended period of up to 21 days, which is crucial for combating the tumor microenvironment by strengthening the activity and functionality of immune cells. Continued monitoring serum levels of IFN- γ and IL-12 for 11 weeks also revealed sustained expression of these cytokines *in vivo*, contributing to the prolonged immune protection conferred by the nanovaccines (Fig. 4G–H). Additionally, the capability of the nanovaccine to elicit a cross-immune response with B cells was investigated following its interaction with T cell responses. After boosting, mouse sera were collected to determine the levels of IgG-OVA using the ELISA method. Despite the designed nanovaccines containing only T cell epitopes, they successfully induced a cross-immune response with B cells after two immunizations, triggering humoral immunity (Fig. S22).

2.5. The tumor therapeutic and prophylactic effects of the nanovaccine

The tumor-suppressive effects of the nanovaccines were tested in the B16-OVA melanoma model, with the nanovaccines or control formulations injected on the 10th, 17th, and 24th days after subcutaneous tumor inoculation. As a result, all mice in the untreated saline group died within 22 days. The groups treated with free antigenic peptides, the physical mixture with equimolar SOCS1 siRNA, and the combination of antigenic peptide with commercial aluminum adjuvants did not show significant inhibition of tumor growth or survival rate benefits. Similarly, the ferritin-fused antigenic peptide vaccine (**FS**) exhibited only moderate inhibition of tumor growth (Fig. 5B and Figs. S23–24). In contrast, the administration of the nanovaccine **siRNA@KFS** yielded the most significant therapeutic effect, with 50 % of mice surviving beyond 35 days (Fig. 5C). Given the crucial role of tumor-infiltrating lymphocytes (TILs) in indicating the immune system's attempts to combat the tumor, immunohistochemical (IHC) analysis was subsequently performed on the collected tumor tissues, showing an increased presence of tumor-infiltrating CD8⁺ cells after the treatment with **siRNA@KFS** (Fig. 5D).

To further evaluate the immune protective effect of the **siRNA@KFS** nanovaccines, a three-week immunization experiment was conducted on mice, with the vaccine administered once a week. 7 days after the final vaccine injection, mice were subcutaneously injected with B16-OVA melanoma cells. Groups receiving saline, free antigen peptide, a physical mixture of free antigen peptide and nucleic acid drug, as well as antigen peptide mixed with aluminum adjuvant, all developed tumors after 23 days within subcutaneous tumor inoculation. In contrast, the fusion protein vaccines with the ferritin structure, namely **FS**, **KFS**, and **siRNA@KFS**, showed no evidence of tumor development (Fig. 5E–F, and Fig. S25), mainly due to the effective activation of immune cells through the enriched antigen epitopes. To further confirm the long-lasting immune responses induced by the nanovaccine, mice were inoculated with tumors 30 days after receiving the vaccine three times. Although both **FS** and **KFS** groups initially exhibited tumor growth, with **KFS** showing slightly better effects than **FS**, all mice developed tumors by the 14th day after tumor inoculation. In contrast, the **siRNA@KFS** group showed no signs of tumor growth within 30 days after tumor inoculation, indicating its long-lasting effectiveness *in vivo* (Fig. 5G and Fig. S24). Furthermore, the proportions of central memory T cells (CD8⁺CD44⁺CD62L^{low}), effector memory T cells (CD8⁺CD44⁺CD62L^{high}), and naive T cells (CD8⁺CD44⁻CD62L⁻) were determined from the collected peripheral blood. As can be seen in Fig. 5H and I, the **siRNA@KFS** group exhibited a greater percentage of memory T cells compared to the **FS** and **KFS** groups, with an activation of 25.1 % effector memory T cells (T_{EM}) and 14.5 % central memory T cells (T_{CM}), providing the organism with a more enduring immune capacity. This enhanced immune response allowed for a rapid reaction following antigen exposure and contributed to sustained anti-tumor responses, potentially preventing tumor recurrence over an extended period. Finally, the *in vivo* biosafety of the nanovaccine was confirmed by the tissue sections from animal specimens, with no toxicity observed in any organs and tissues (Fig. S27). Furthermore, biochemical tests for blood urea (Fig. S28) revealed no abnormalities in renal function indicators.

2.6. Application of nanovaccine in authentic tumor antigens

Faced with the limited applicability of requiring customized tumor-specific antigens, more tumor-associated antigens with certain immunogenicity due to overexpression or mutation have been discovered. In this context, the overexpressed glycoprotein 100 in melanoma tissue (gp100₂₅₋₃₃) was selected as the second candidate antigen to demonstrate the programmability and adaptability of our nanovaccine platform for extended application in cancer therapy [52–54]. Therefore, a new light chain ferritin-based nanovaccine was engineered, in which the C-terminal fusion antigen was replaced by the T-cell epitope of the melanoma neoantigen peptide gp100. After comprehensive characterizations of the nanovaccine, similar structures and functionality as **KFS** were revealed (Figs. S30–S36). On the 7th day, mice were subcutaneously immunized with various formulations, including free antigenic peptide, antigenic peptide physically mixed with SOCS1 siRNA, antigenic peptide supplemented with commercial aluminum adjuvant, the vaccine simply fused with ferritin (**Fgp100**), and **KFgp100** without siRNA as control. Subsequently, mice were subcutaneously injected every 7 days after B16F10 cell inoculation, resulting in obvious tumor

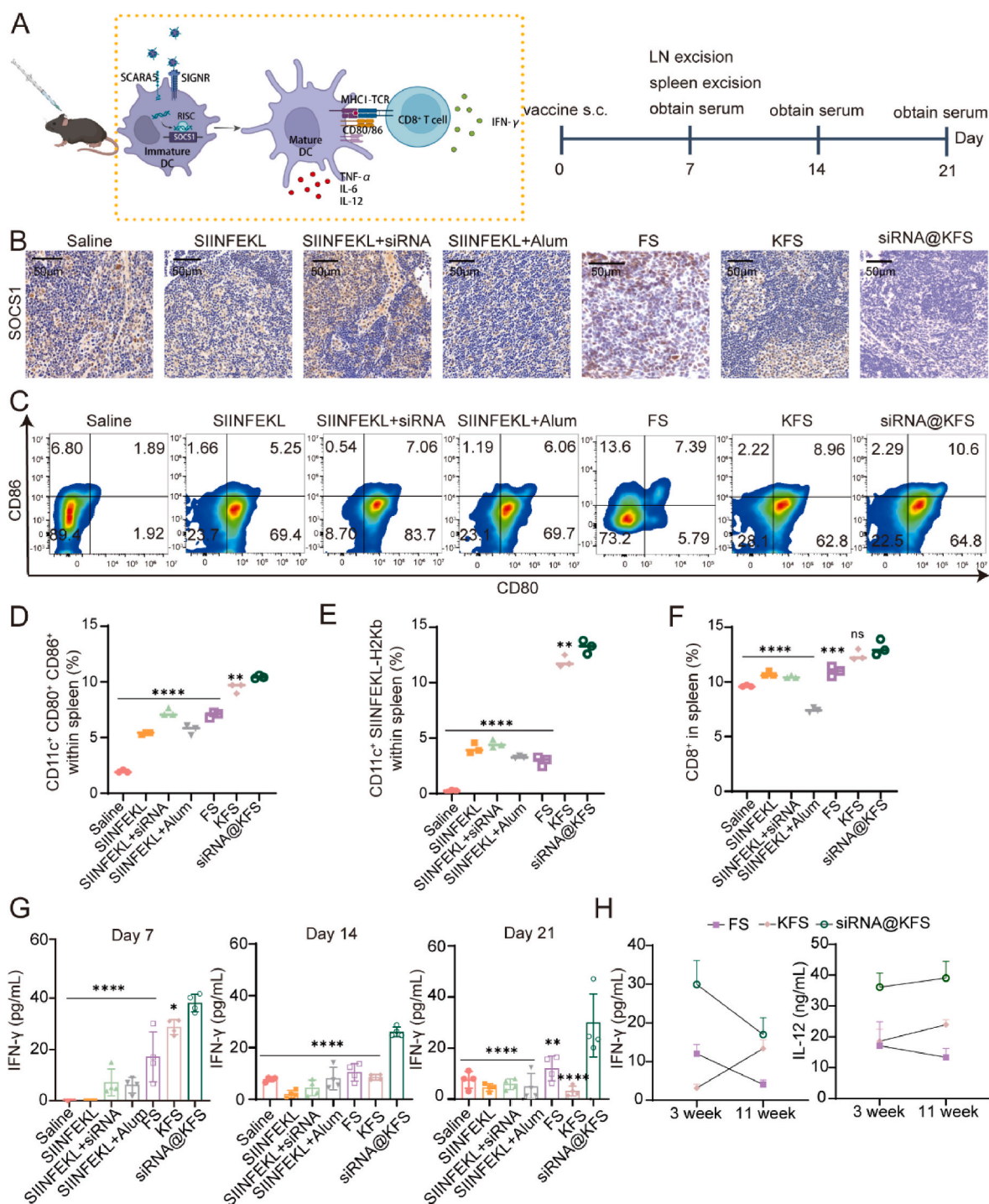


Fig. 4. *In vivo* immune stimulation by the nanovaccines. (A) Schematic illustration and the timeline of the experimental design to evaluate the *in vivo* immune responses triggered by anti-SOCS1 siRNA-loaded KFS nanovaccine. (B) Immunohistochemical analysis of the SOCS1⁺ cells in tumor draining lymph nodes of mice that treated with nanovaccines or the control formulations, scale bars 50 μ m. (C,D) The DCs expressing CD80 or CD86 from spleen (n = 3). (E) Percentages of the OVA (SIINFEKL)-presenting DCs (n = 3) assessed by flow cytometry. (F) The frequency of CD8⁺ T cells measured by flow cytometry after the vaccination with the indicated formulations (n = 3) (G,H) Levels of IFN- γ and IL-12 in the serum at different time intervals after the vaccination. Representative data are shown and expressed as the mean \pm s.d. Statistical significance was estimated by one-way ANOVA: *p<0.05, **p<0.01, ***p<0.001, ****p<0.0001. ns, not significant.

suppression from the nanovaccine **siRNA@KFgp100**, with its survival rate remained at 30 % after 60 days (Fig. 6B–D), significantly extended compared to other groups. Moreover, due to the strong metastatic and invasive abilities of B16F10, the nanovaccine effectively inhibited tumor metastasis to the lung (Fig. 6E). Additionally, infiltrating T cells in B16F10 tumor tissues were analyzed using IHC, showing the highest number of tumor-infiltrating lymphocytes (TILs) from the group treated

with **siRNA@KFgp100** (Fig. 6F). These findings demonstrate the interchangeable ability of the antigen that fused into the nanovaccine platform, which can potentially be expanded to various tumor-specific antigens (TSA) or tumor-associated antigens (TAA) for different cancer immunotherapy.

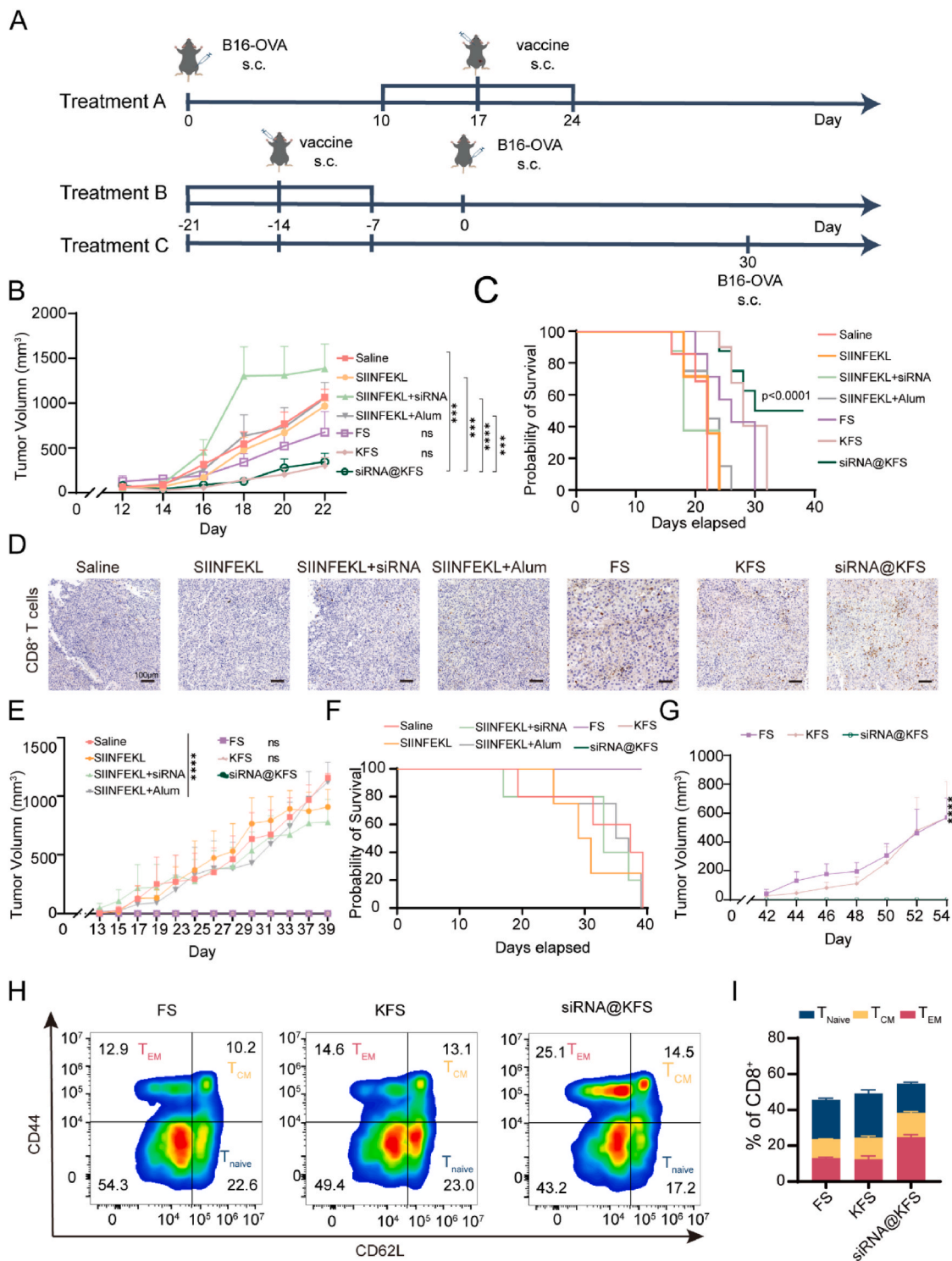


Fig. 5. *In vivo* therapeutic and prophylactic effects of nanovaccine siRNA@KFS towards B16-OVA tumors. (A) Schematic timeline of the experimental design. Treatment A involves initial establishment of a subcutaneous B16-OVA mice model and the vaccine administration when the tumor grown to larger than 50 mm³. Treatment B and C involves administering the vaccine three times, followed by tumor inoculation after 0 and 30 days, respectively. (B) Average tumor growth curves for B16-OVA tumors on mice after various treatments as indicated (n = 6). Growth curves represent means ± s.e.m. (C) Morbidity-free survival of different groups of B16-OVA-bearing mice after various treatments. Survival curves were obtained using the Kaplan-Meier method and compared by the log-rank test, ****p < 0.0001 (n = 6). (D) Immunohistochemical analysis of CD8⁺ T-cell infiltration in B16-OVA tumors from mice that treated with nanovaccines or the control formulations, scale bars, 100 μm. (E) Average tumor growth curves for B16-OVA tumors on mice after the various treatments as indicated in Treatment B (n = 5). Growth curves represent means ± s.e.m. (F) Morbidity-free survival of different groups of B16-OVA-bearing mice after various treatments. Survival curves were obtained using the Kaplan-Meier method and compared by the log-rank test (n = 5). (G) Average tumor growth curves for B16-OVA tumors on mice after the various treatments as indicated in Treatment C (n = 5). Growth curves represent means ± s.e.m. (H,I) T_{EM} and T_{CM} in the peripheral blood analyzed by flow cytometry (gated on CD8⁺ T cells) on day 60 after final vaccination.

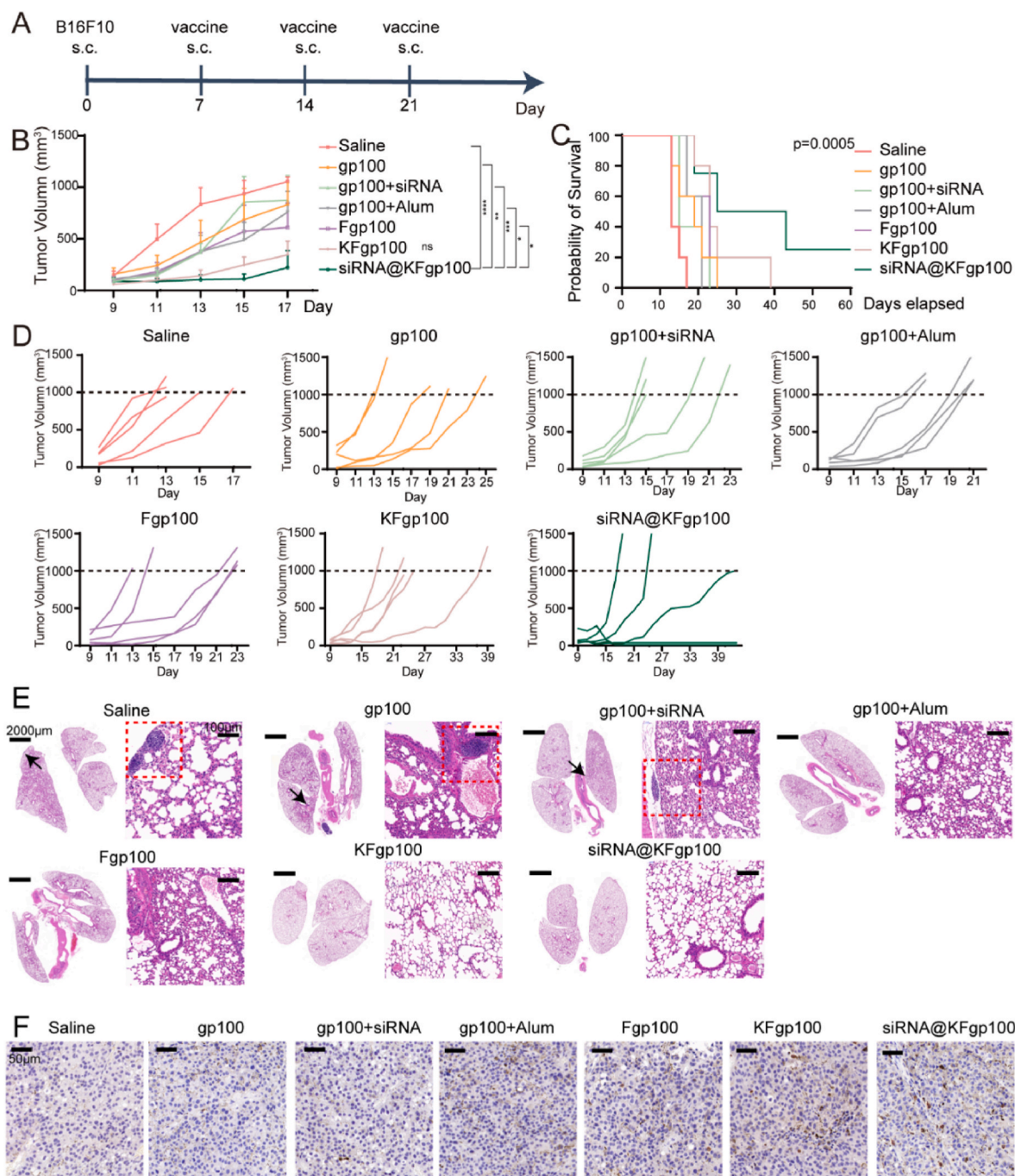


Fig. 6. *In vivo* therapeutic effects of nanovaccine siRNA@KFgp100 towards B16F10 tumors. (A) Schematic timeline of the experimental design. (B) Average tumor growth curves for B16F10 tumors on mice after various treatments as indicated ($n = 5$, biologically independent mice for each group). Growth curves represent means \pm s.e.m. (C) Morbidity-free survival of different groups of B16F10-bearing mice after various treatments. Survival curves were obtained using the Kaplan-Meier method and compared by the log-rank test, $***p < 0.0001$ ($n = 5$). (D) Individual tumor growth curves. (E) H&E staining of lungs collected from the treated mice. The black arrows point to tumor metastases (deep-stained regions) in lungs. Scale bars, 2 mm. (F) IHC analysis of CD8⁺ T-cell infiltration in B16F10 tumors from mice treated with nanovaccines or the control formulations, Scale bars, 50 μ m.

3. Discussions

Cancer vaccines can be divided into three types based on the source of tumor antigens: protein/peptide vaccines, genetic vaccines, and cell-based vaccines (DC vaccines and whole-tumor-cell vaccines) [55]. These types of vaccines have demonstrated certain clinical efficacy, benefiting from relatively mature preparation processes and offering potential for personalized customization. Peptide vaccines lead in the number of clinical trials compared to other types of cancer vaccines. Especially

following the recent breakthroughs in genomics, data science, and tumor immunology, neoantigens with innate immunogenicity can be easily obtained after comprehensive sequencing and HLA affinity testing, providing a straight forward pathway for personalized peptide vaccine [56–58]. However, when used as standalone treatments, the objective response rate of peptide vaccines remains disappointingly low [59–62], largely due to issues such as rapid clearance and low immunogenicity [8]. To overcome these challenges, various delivery systems and adjuvants have been developed. Compared to other delivery

vectors, ferritin has emerged as a promising platform because of its excellent antigen protection and biocompatibility [36–40].

In the current study, human ferritin light chain (L-Ferritin) was chosen as the backbone for the fusion protein vector. Compared to ferritin from other species, such as *H. pylori* and *E. coli* [35], human ferritin has higher homology and immune tolerance, which minimizes the inflammatory responses that may lead to adaptive immune attenuation. Compared to human ferritin heavy chain, the light chain of ferritin exhibits a higher affinity for SCARA5 and DC-SIGN receptors on APCs, thereby improving vaccine targeting efficiency. In addition, unlike the heavy chain, the ferritin light chain does not bind to Tfr1, lacks iron oxidation capabilities, and is less involved in iron metabolism, making it a safer carrier for cancer vaccines. Subsequently, the nano-vaccine was designed by fusing an interchangeable tumor antigen and the cationic KALA peptide to the C- and N-terminus of L-ferritin, respectively. As a result, the fusion of KALA peptide increased the self-aggregation of ferritin from 8-mer to 40-mer, leading to a particle size of 25 nm, which significantly facilitates its draining into lymph node [63]. Meanwhile, the higher antigen density upon 40-mer aggregation enhanced the chances of DC binding to antigens, further promoting DC uptake and subsequently raising the antigen presentation rate to 29.7 %.

Furthermore, co-delivery of siRNA was achieved through the binding with the positively charged KALA peptide. Specifically, SOCS1 siRNA was used here to restore Janus kinase (JAK) activity, allowing downstream STAT signaling to continue and alleviating immune suppression in DCs, thus promoting DC maturation. In contrast to adjuvants based on pathogen-associated molecular pattern molecules (PAMPs), using SOCS1 siRNA fundamentally avoided risks such as activating humoral immunity and inducing strong inflammatory responses, which can compromise adaptive immunity [63–65]. The current strategy effectively facilitated DC-T cell crosstalk through several approaches: the DC-targeting effect by ferritin light chain, enhanced DC uptake by KALA peptide, and promoted DC maturation by SOCS1 siRNA, thus, enhancing the expression of co-stimulatory molecules (CD80/86) to 15.2 %, and elevating related cytokines (TNF- α , IL-6, IL-12) expression. These processes significantly activated T cell functions, bridging innate and adaptive immunity [66,67]. Meanwhile, the secreted cytokines promoted the differentiation of T cells into memory T cells, with active effector memory T cells at 25.1 % and central memory T cells at 14.5 % even 60 days post-vaccination. This prolonged the immuno-protective effects and reduced the need for frequent administrations.

Compared to other nanoparticle vaccines that consist of separate components for antigen, adjuvant, and carrier, our all-in-one fusion protein-based nanovaccine presents a novel approach. Validating its adaptability for a broader spectrum of antigens is essential. Given that the typical length of HLA-I antigenic fragments ranges from 8 to 11 amino acids [68], we tested two T-cell epitope peptides: tumor-specific antigen (OVA) and tumor-associated antigen (gp100). These nanovaccines maintained stable structures and effectively loaded and protected siRNA, significantly inhibiting tumor growth and prolonging survival. Notably, siRNA@KFgp100 was examined in a high invasive and metastatic B16F10 tumor model, demonstrating a strong preventive effect on lung metastasis. Their high receptivity suggests substantial potential for clinical applications.

Vaccine safety is critically important, particularly considering serious adverse reactions reported for COVID-19 vaccines, such as vaccine-induced immune thrombocytopenia (VITT) and autoimmune diseases. Although the detailed mechanisms remain unclear, adenoviral vectors have been linked to some VITT cases, suggesting a direct role of vaccine vector in these adverse reactions [69,70]. In this study, homologous ferritin was used as the vaccine vector instead of a viral or synthetic vector, offering significant safety advantages. For example, *Helicobacter pylori* ferritin based COVID-19 vaccine has been developed by the Walter Reed Army Institute of Research [71,72]. Apart from injection site reactions such as pain, redness, swelling, fever, and fatigue, no other severe adverse effects have been reported [73]. However,

excess ferritin, even its light chains, can potentially lead to iron overload and associated oxidative stress. Thus, establishing a safe dosage for ferritin-based vaccines is crucial for future research. Besides vector issues, off-target risks associated with RNAi technology also remain a challenge. Therefore, various strategies were employed in this study to mitigate these risks, including using siRNA sequences that are homologous to the target mRNA and applying low siRNA doses (50 pmol *in vitro* and 0.231 nmol/mouse *in vivo*) to reduce nonspecific binding. Additionally, the lymph node-targeting effect of the nanovaccine significantly enhanced siRNA accumulation in APCs, thereby reducing off-target possibilities. However, to further eliminate off-target risks, whole-genome expression analysis can be conducted for risk assessment [74], while evaluating impacts on other immune and physiological pathways following the temporary silencing of the SOCS1 gene in tumor-bearing mice.

4. Conclusions

In the current work, we have developed a novel nano-vaccine based on the human ferritin light chain delivery platform. By fusing with antigen and the positively charged KALA peptide, this peptide nano-vaccine is also capable of co-delivering immunosuppressive regulatory siRNA. The higher aggregation degrees of the fusion protein compared to ferritin, along with its affinity to SCARA5 receptor and SIGNR of dendritic cells and membrane-penetrating property, greatly promoted the draining and accumulation of the nano-vaccine in lymph nodes, and facilitated its uptake by antigen-presenting cells (Figs. 1–2). Owing to the successful delivery of SOCS1 siRNA, the maturation of immature DCs was significantly promoted both *in vitro* and *in vivo*, leading to elevated levels of antigen presentation, consequently enhancing CD8⁺ T cell activity and sustaining immune responses (Figs. 3–4). With interchangeable antigens in the fusion protein, the nano-vaccine has been demonstrated effective inhibition of tumor growth in both tumor-specific antigen (SIINFEKL) and tumor-associated antigen (gp100) models. Moreover, the higher number of memory T cells induced by the nano-vaccine avoided the need for frequent administrations as in other vaccines, while still providing enduring protective effects (Figs. 5–6) for tumor prevention.

In summary, this DCs-targeting ferritin light chain-based nano-vaccine with the ability of simultaneous delivery of antigen and siRNA, demonstrated excellent efficacy in promoting DCs maturation and enhancing T cell activity without the use of any adjuvants. This platform provided a new strategy for both cancer treatments and prevention, opening an avenue for the design of personalized cancer vaccines.

5. Experimental methods

5.1. Animals

C57BL/6 mice (6 weeks old) were purchased from GemPharmatech Animal Technology Co., Ltd. All animals were maintained at 25 °C, 40 % relative humidity, with free access to food and water, and a 12 h light/dark cycle. All animal studies were conducted in accordance with the Animal Research Committee of Jiangnan University school of Medicine, and all the operation procedures were conducted according to National Institutes of Health Guide. The ethical approval numbers for the animal experiments are JN.No20230615c0961001[324] and JN.No20230330c0510801 [104].

5.2. Cell cultures

The mouse melanoma B16F10 and B16F10 cell line stable expressing ovalbumin (B16-OVA) was established by lentiviral transfection. Cell lines and the mouse macrophage RAW 264.7 and mouse dendritic cell DC2.4 were purchased from the American Type Culture Collection. The mouse melanoma B16-OVA cells and mouse Dendritic cell line DC2.4

were maintained in RPMI1640 medium supplemented with 10 % fetal bovine serum (FBS), and 100 units per mL penicillin and 100 units per mL streptomycin at 37 °C in 5 % CO₂. The mouse B16F10 cell lines were maintained in DMEM/F12 medium supplemented with 100 units per mL penicillin and 100 units per mL streptomycin at 37 °C in 5 % CO₂. The mouse RAW 264.7 cell lines were maintained in DMEM medium supplemented with 10 % fetal bovine serum (FBS), and 100 units per mL penicillin and 100 units per mL streptomycin at 37 °C in 5 % CO₂.

Murine BMDCs were isolated from femurs and tibiae of C57BL/6 mice, and maintained in RPMI1640 medium supplemented with 10 % FBS, penicillin G (100 U/mL) and streptomycin (100 g/mL) at 37 °C in 5 % CO₂. Recombinant mouse GM-CSF (20 ng/mL) and IL-4 (10 ng/mL) were added to induce cell differentiation. The medium was half-replaced every 2 days. On the 7th day of culture, the medium was gently pipetted; immature BMDCs cells that were suspended in the medium and loosely adhered to the flask were all collected for further use.

CD3⁺ T cells were obtained from spleen of C57BL/6 mice. Cell extraction was conducted using the Beaver Biosciences Inc. kit following the instructions of the supplier. CD3⁺ T cells were cultured in RPMI 1640 medium with 10 % FBS, penicillin G (100 U/mL), and streptomycin (100 g/mL). Cells were maintained in a humidified incubator at 37 °C with 5 % CO₂.

5.3. Cloning, expression and purification of the fusion proteins

The wild-type human light chain ferritin (5–154 aa) was truncated. KALA peptide (WEAKLAKALAKALAKHLAKALAKALKA) was attached to its N-terminus. At its C-terminus, the T-cell epitope SIINFEKL from Ovalbumin (OVA) was connected via a (G₄S)₃ linker. After being designed for *E. coli* codon preference, the gene was synthesized by Azenta Technologies. The fragment was cloned into the pET28α(+) plasmid using *Bam*HI and *Xho*I restriction enzyme sites. The resulting plasmid was transformed into BL21(DE3) *E. coli*, and single colonies were picked. The cultures were grown overnight at 37 °C in LB medium containing 50 µg/mL kanamycin. The culture was then expanded in 300 mL of Lysogeny Broth medium (LB) until the OD₆₀₀ reached 0.6. Induction of protein expression was carried out overnight at 16 °C with a final concentration of 0.3 mM IPTG. The bacterial culture was harvested and subjected to high-pressure homogenization in PB buffer (20 mM Na₃PO₄, 0.5 M NaCl, pH 7.4). The supernatant was collected after centrifugation, and treated with the broad-spectrum nuclease Benzonase Nuclease (Sigma) at a dosage of 4 U/mL at 4 °C overnight to remove extra nucleic acids. After centrifugation at 4 °C for 45 min to remove the precipitate, the supernatant was collected as the initial protein sample. Nickel-affinity chromatography was then performed to purify the KFS protein through gradient elution. The proteins F, KF, and FS were amplified by PCR using the pET28α(+)-KFS plasmid as a template. They were then cloned into the pET28α(+) plasmid using the same *Bam*HI and *Xho*I restriction enzyme sites, and expressed and purified under the same conditions as KFS. KFgp100 is derived from KFS by replacing the C-terminus OVA antigen with gp100₂₅₋₃₃(EGPRNQDWL), which was synthesized by Azenta Technologies. The fragment was cloned into the pET28α(+) plasmid using *Bam*HI and *Xho*I restriction enzyme sites, resulting in pET28α(+)-KFgp100, which was then transformed into BL21(DE3) *E. coli*. Subsequently, amplification conditions and induction expression conditions were the same as for KFS. Fgp100 was generated by PCR using the pET28α(+)-KFgp100 plasmid as a template. The fragment was then cloned into the pET28α(+) plasmid using the same restriction enzyme sites, and expressed and purified under the same conditions as KFgp100. Endotoxin was removed from all of the proteins with a ToxinEraser endotoxin removal kit (GenScript). The amount of endotoxin is less than 0.1 EU/mL.

5.4. Characterization and in vitro cytotoxicity assessment of the fusion protein

The sizes and zeta potentials of the different proteins were measured with a Zetasizer Nano ZS (Malvern Instruments). The native-state apparent molecular weight of the fusion protein was determined by Native PAGE, followed by size exclusion chromatography using a Superose 6 Increase column on the AKTA Pure system. The protein aggregation was assessed using high-performance liquid chromatography with size exclusion chromatography (HPLC-SEC). A TSK G3000SWXL (7.8 × 300 mm) column was used for separation, with a mobile phase consisting of 0.1 M sodium sulfate and 0.1 M sodium phosphate buffer at pH 6.7. The flow rate was maintained at 0.5 mL/min, and the column temperature was set to 30 °C. Detection was performed at UV wavelengths of 220 nm and 280 nm using a Waters 2695 HPLC system, equipped with a 2487 UV detector and controlled by Empower software with GPC modules. The cytotoxicities of fusion protein were measured by a well-established MTT assay. Generally, BMDCs incubated with KFS at various concentrations were seeded in a 96-well plate at a density of around 5 × 10⁴ cells per well for 24 h. Then, a standard MTT assay was used to determine the relative cell viability.

5.5. Preparation and characterization of nanovaccine siRNA@KFS

The siRNA@KFS was obtained by incubating the KFS and SOCS1 siRNA at an N/P molar ratio of 10 at RT for 15 min. The N/P ratio was calculated as follows: 1 mol of P corresponds to 1/42 mol of siRNA, and 1 mol of N corresponds to 1/7 mol of KFS. The complex was tested for stability or used for silencing experiments without further purification. For stability test, the siRNA@KFS was incubated in 50 % mouse serum at 37 °C. The siRNA in the complex was labelled with Cy5 (Gene Pharma Technologies). Aliquots of 5 µL (10 pmol siRNA equivalent) was collected at various time intervals and probed on a 2 % agarose gel. To validate the nanovaccine's resistance to nucleic acid degradation, free nucleic acid was used as a control. After with 5U Benzonase (Sigma) for 1 h at 37 °C, gel electrophoresis was performed to assess the integrity of siRNA. The gel images were obtained using a multifunctional gel image analysis system (Tanon MINI SPACE 3000). The morphological changes before and after loading siRNA onto the fusion protein KFS were characterized by transmission electron microscopy. 5 µL samples (0.5 mg mL⁻¹) were applied to glow-discharge electron microscopy grids covered by a thin layer of continuous carbon film and stained with 2 % (w/v) uranyl acetate. Negatively stained grids were imaged on an H-7650 microscope (HITACHI) operating at 120 kV.

5.6. In vitro cellular uptake and intracellular localization

To assess the cellular uptake, 2 × 10⁵/mL BMDCs, RAW 264.7 were plated in 24-well dishes (NEST) and stimulated with Cy5-labelled antigen peptide (10 µM), Cy5-labelled KFS (10 µM) or Cy5-labelled siRNA (50 nM), KFS loaded with equal amounts of Cy5-labelled siRNA for several time intervals. Then the cells were harvested for flow cytometry analysis (Cytoflex A00-1-1102). In order to track the intracellular path of the nanovaccines, RAW 264.7 cells were treated with the siRNA@KFS for 1, 2 or 4 h, respectively, and then washed with PBS for three times. The lysosome and nuclei were stained with Lyso-tracker green (200 nM) and DAPI, respectively. After being washed with PBS, the cells were observed with a laser scanning confocal microscope (Nikon Ti2-E). In order to verify whether there is receptor preference for endocytosis, 1 × 10⁵ HEK293 and BMDCs were seeded in confocal dishes. Cy5-labelled KFS (10 µM) was treated for 30 min, washed three times with 1 × PBS, and the cell membrane and nucleus were stained with DiO dye and DAPI respectively, then observed using a confocal microscope.

5.7. Evaluation of gene silencing activity against *SOCS1* gene in BMDCs

Anti-*SOCS1* siRNA: 5'-GAGAACCUGGCGCGCAUCCUCUUA-3', 5' UAAGAGGGAUGCGGCCAGGUUCUC-3') was synthesized and obtained from Gene Pharma Technologies. Immature BMDCs (5×10^5 cells) were seeded onto a 12-well culture plate (NEST) and stimulated with the nanovaccine (**siRNA@KFS**). The nanovaccine consisted of the fusion protein **KFS** which loaded with 50 nM anti-*SOCS1* siRNA, with an N/P ratio of 50, i.e., a protein concentration of 6.1 μ M incubated for 4 h at 37 °C in 0.5 mL of serum-free RPMI1640. After the incubation, 0.5 mL of fresh culture medium containing 20 % FBS was added to the cells, followed by a further incubation for 20 h. Free siRNA (50 nM), antigen peptide (6.1 μ M), and physically mixed antigen peptide (6.1 μ M) and siRNA (50 nM), and vehicle fusion protein **KFS** (6.1 μ M) as control, were incubated for 24 h in 1.0 mL RPMI1640 containing 10 % FBS. After the post-treatment, the cells were collected and used for the evaluation for RNA isolation by Trizol method. Performing RT-PCR using One Step RT-qPCR Probe Kit (Yeasen) and following the manufacturer's instructions provided. Quantitative polymerase chain reaction (PCR) was performed with a Bio-Rad CFX System in 20 μ L aliquots of reaction mixtures containing cDNA, appropriate pairs of primers and SYBR Green Realtime PCR Master Mix (Yeasen). *Socs1*, *Jak1* and *Stat1* level was calculated by the comparative CT method using β -actin as endogenous housekeeping genes. The primer pairs are showed in [Supplementary Information Table S5](#). Proteins were extracted by lysing cells on ice with RIPA buffer (Beyotime) containing protease inhibitors. The protein concentrations were determined using a BCA protein assay kit (Yeasen). Protein lysates (20 μ g/lane) were separated using 10 % sodium dodecyl sulfate-polyacrylamide gels (SDS-PAGE) electrophoresis and transferred onto polyvinylidene fluoride membranes (Merck). The membranes were subsequently blocked for using 5 % skim milk for 1 h and incubated with primary antibodies overnight at 4 °C. Subsequently, the membranes were incubated with respective secondary antibodies (rabbit) at room temperature for 1 h. After washing thrice with PBST, the signals were detected on a Tanon chemiluminescence image analysis system. All the antibodies used are listed in [Table S7](#).

5.8. *In vitro* DC activation and cross-presentation

Immature BMDCs (5×10^5 per mL) were plated onto 12-well dishes (NEST) and stimulated with **siRNA@KFS**, **KFS**, **FS**, free anti-*SOCS1* siRNA or free antigen peptide SIINFEKL and the mixture of peptide and siRNA at 37 °C for 24 h. BMDCs were harvested and re-suspended in PBS buffer. For DC activation analysis, BMDCs were stained with anti-CD11c (0.25 μ g per 100 μ L), anti-CD80 (1.0 μ g per 100 μ L), anti-CD86 (1.0 μ g per 100 μ L) and anti-SIINFEKL-H-2Kb (0.125 μ g per 100 μ L) antibodies for 30 min on ice. The BMDCs were then washed with FACS buffer and analyzed using flow cytometry. The supernatant was collected and analyzed for TNF- α , IL-6 and IL-12 using an ELISA kit (Thermo Fisher Scientific Inc.) according to the manufacturer's instructions.

5.9. T cell proliferation and activation

Immature BMDCs (5×10^5 per mL) were plated onto 12-well dishes (NEST) and stimulated with **siRNA@KFS**, **KFS**, **FS**, free anti-*SOCS1* siRNA or free antigen peptide SIINFEKL and the mixture of peptide and siRNA at 37 °C for 24 h. BMDCs were harvested and re-suspended in PBS buffer for further use. The proliferation of CD3⁺T cells was determined by CFSE staining (Yeasen Biotechnology). Before coculturing with DC, T cells were incubated with 5 μ M CFSE for 15 min at 37 °C. The cells were then washed three times with PBS to remove excess CFSE. After co-culturing T cells and treated DC for 24 h, T cells were separated and quantified by flow cytometry with under the excitation of 488 nm. The supernatant was collected and analyzed for TNF- α , IL-6 and IFN- γ using ELISA kits (Thermo Fisher Scientific Inc.) according to the

manufacturer's instructions.

5.10. Biodistribution of *KFS*

To investigate their biodistribution, **KFS** were labelled with Cy5 (5 nmol per mouse) and antigen peptides SIINFEKL were also labelled with Cy5 (5 nmol per mouse). Following the standard protocol and injected at the tail base of the mice. After different time intervals, major organs, such as the heart, liver, spleen, lung, kidney, inguinal lymph nodes were collected and examined using an *in vivo* optical imaging Nsystem (IVIS Spectrum, PerkinElmer). Analysis of fluorescence intensity of lymph nodes and organs was performed with Living Image 4.1 software.

5.11. *In vivo* immunology research

C57BL/6 mice were randomly divided into 7 groups of six mice per treatment group and treated with Saline, **siRNA@KFS** (5 nmol **KFS**, containing anti-*SOCS1* siRNA 0.231 nmol per mouse), **KFS** (5 nmol per mouse), **FS** (5 nmol per mouse), antigen peptide SIINFEKL (5 nmol per mouse), the physical mixture (5 nmol peptides and 0.231 nmol anti-*SOCS1* siRNA) or antigen peptide combined with aluminum adjuvant (5 nmol peptides and the dosage of aluminum adjuvant is three times the mass of the antigen peptides) by subcutaneous injection on day 0. Three mice were randomly sacrificed from each group and inguinal lymph nodes and spleens were harvested. The spleens were gently crushed and passed through a 40 μ m cell strainer to obtain isolated cells. After red blood cell lysed the cells were then washed with cold FACS buffer and suspended in FACS buffer stained by anti-CD11c (0.25 μ g per 100 μ L), anti-CD80 (1.0 μ g per 100 μ L), anti-CD86 (1.0 μ g per 100 μ L), anti-SIINFEKL/H-2Kb (0.125 μ g per 100 μ L), anti-CD3 (0.5 μ g per 100 μ L) and anti-CD8a (0.5 μ g per 100 μ L) antibodies for 30 min on ice. Flow cytometry was then performed on the stained cell suspension. The specific information regarding the flow cytometry antibodies is listed in [Table S6](#). The inguinal lymph nodes were fixed in 4 % paraformaldehyde/PBS for 12 h and placed into a 30 % sucrose/PBS solution overnight at 4 °C. The fixed tissues were cut into 6 μ m-thick sections with a cryostat. The sections were processed with IHC treated with mouse anti-*SOCS1* antibody (Servicebio Technology) overnight at 4 °C, with HRP-conjugated secondary antibody, and with DAB. The tissue sections were counterstained with hematoxylin for nucleus visualization. Blood samples were collected from each group of mice every 7 days through the submandibular vein, and serum was obtained for ELISA detection of IFN- γ , IL-12 and IgG-OVA.

5.12. *In vivo* cancer therapeutic studies

To assess the *in vivo* therapeutic efficacy of the nanovaccine, C57BL/6 mice were inoculated subcutaneously with 2×10^5 B16-OVA melanoma cells into the right rear side of the back of mice on day 0. Tumors were allowed to grow for 10 days and these tumor-bearing mice were randomly divided into seven groups. On day 10, day 17 and day 24, mice were subcutaneously vaccinated with either Saline, **siRNA@KFS** (5 nmol **KFS**, containing anti-*SOCS1* siRNA 0.231 nmol per mouse), **KFS** (5 nmol per mouse), **FS** (5 nmol per mouse), antigen peptide SIINFEKL (5 nmol per mouse), the physical mixture (5 nmol peptides and 0.231 nmol anti-*SOCS1* siRNA) or antigen peptide combined with aluminum adjuvant (5 nmol peptides and the dosage of aluminum adjuvant is three times the mass of the antigen peptides). To ensure the programmability of the nanovaccine, another tumor model was established. C57BL/6 mice were inoculated subcutaneously with 2×10^5 B16F10 melanoma cells into the right rear side of the back of mice on day 0. Tumors were allowed to grow for 7 days and these tumor-bearing mice were randomly divided into 7 groups. On day 7, day 14 and day 21 mice were subcutaneously vaccinated with either saline, **siRNA@KFgp100** (5 nmol **KFgp100**, containing anti-*SOCS1* siRNA 0.231 nmol per mouse), **KFgp100** (5 nmol per mouse), **Fgp100** (5 nmol per mouse), antigen

peptide gp100₂₅₋₃₃ (5 nmol per mouse), the physical mixture (5 nmol peptides and 0.231 nmol anti-SOCS1 siRNA) or antigen peptide combined with aluminum adjuvant (5 nmol peptides and the dosage of aluminum adjuvant is three times the mass of the antigen peptides). Tumors were monitored every other day using calipers in three dimensions. Tumor volumes were calculated using formula $V = 0.5 \times L \times S^2$, where L and S are the larger and smaller diameters, respectively. Mice were euthanized when the tumor volumes reached 1500 mm³. The tumor tissues were fixed in 4 % paraformaldehyde/PBS for 12 h and placed into a 30 % sucrose/PBS solution overnight at 4 °C. The fixed tissues were cut into 6 μm-thick sections with a cryostat. The sections were processed with IHC treated with mouse anti-CD8a antibody (Servicebio Technology) overnight at 4 °C, with HRP-conjugated secondary antibody, and with DAB. The tissue sections were counterstained with hematoxylin for nucleus visualization. Blood samples were collected from the submandibular vein of mice in both the siRNA@KFS group and the untreated group, and serum was obtained for blood biochemical tests.

5.13. Prophylactic and therapeutic studies with OVA-based nanovaccines

For the prophylactic study, different vaccines were subcutaneously injected into the female C57BL/6 mice of each group at intervals of one week for three times. 7 days or 30 days after the final vaccination, the vaccinated mice were subcutaneously challenged with 5×10^5 B16-OVA cells. The tumor volume was measured with a caliper every other day and calculated according to following the formula: $V = 0.5 \times L \times S^2$, where L and S are the larger and smaller diameters, respectively. Mice were euthanized when the tumor volume reached 1500 mm³.

5.14. Analysis of memory T cells

The mice were administered with FS, KFS or siRNA@KFS on day 60 after the final vaccination, the peripheral blood was analyzed by flow cytometry. The cells were stained with anti-mouse CD8α (0.25 μg in 100 μL), anti-mouse CD44 (0.25 μg in 100 μL) and anti-mouse CD62L (0.25 μg in 100 μL) antibodies for 30 min on ice and analyzed by flow cytometry. Central memory T cells were defined as CD8⁺CD44⁺CD62L^{high} and effector memory T cells were defined as CD8⁺CD44⁺CD62L^{low}. The specific information regarding the flow cytometry antibodies is listed in Table S6.

5.15. Gating strategies

The detailed gating strategies for all flow cytometry measurements are included in the supplementary Figures.

5.16. Statistical analysis

The methods for statistical analysis and samples sizes (n) are specified in the results section or figure legends for all of the quantitative data. All values are reported as means ± s.d. or means ± s.e.m. with the indicated sample size. No samples were excluded from analysis. All relevant statistical tests are two-sided. P values less than 0.05 were considered statistically significant. All animal studies were performed after randomization. Statistics were performed using Matlab software.

CRediT authorship contribution statement

Jun Wu: Writing – original draft, Methodology, Formal analysis, Data curation, Conceptualization. **Jing Liang:** Methodology, Formal analysis, Data curation. **Sichen Li:** Methodology, Data curation. **Jinjin Lu:** Data curation. **Yi Li:** Validation. **Bin Zhang:** Data curation. **Min Gao:** Writing – review & editing, Resources. **Juan Zhou:** Writing – review & editing, Resources. **Yan Zhang:** Writing – review & editing, Supervision, Funding acquisition, Conceptualization. **Jinghua Chen:**

Writing – review & editing, Funding acquisition, Conceptualization.

Ethics approval and consent to participate

The experimental protocol concerning animals used in this work was approved by the Jiangnan University Animal Care and Use Committee, JN.No20230615c091001 [323] and JN.No20230330c0510801 [104].

Funding

This work was supported by National Key R&D Program of China (2021YFC2103100), National Natural Science Foundation of China (22008090), Natural Science Foundation of Jiangsu Province (BK20180625), Postgraduate Research & Practice Innovation Program of Jiangsu Province [KYCX22_2329].

Declaration of competing interest

The authors declare the following financial interests/personal relationships which may be considered as potential competing interests: Jinghua Chen reports financial support was provided by National Key R&D Program of China. Yan Zhang reports financial support was provided by National Natural Science Foundation of China. Yan Zhang reports financial support was provided by Natural Science Foundation of Jiangsu Province. Jun Wu reports financial support was provided by Postgraduate Research & Practice Innovation Program of Jiangsu Province. Other authors declare that they have no known competing financial interests or personal relationships that could have appeared to influence the work reported in this paper.

Appendix A. Supplementary data

Supplementary data to this article can be found online at <https://doi.org/10.1016/j.bioactmat.2024.12.029>.

References

- [1] Y. Yang, Cancer immunotherapy: harnessing the immune system to battle cancer, *J. Clin. Invest.* 125 (2015) 3335–3337.
- [2] J.C. Del Paggio, Cancer immunotherapy and the value of cure, *Nat. Rev. Clin. Oncol.* 15 (2018) 268–270.
- [3] O.K. Dagher, R.D. Schwab, S.K. Brookens, A.D. Posey, Advances in cancer immunotherapies, *Cell* 186 (2023) 1814–e1.
- [4] I. Le, S. Dhandayuthapani, J. Chacon, A.M. Eiring, S.S. Gadad, Harnessing the immune system with cancer vaccines: from prevention to therapeutics, *Vaccines* 10 (2022) 816.
- [5] M. Saxena, S.H. van der Burg, C.J.M. Melief, N. Bhardwaj, Therapeutic cancer vaccines, *Nat. Rev. Cancer* 21 (2021) 360–378.
- [6] J. Nam, S. Son, K.S. Park, W. Zou, L.D. Shea, J.J. Moon, Cancer nanomedicine for combination cancer immunotherapy, *Nat. Rev. Mater.* 4 (2019) 398–414.
- [7] J.T. Schiller, D.R. Lowy, I.H. Frazer, O.J. Finn, E. Vilar, H.K. Lyerly, et al., Cancer vaccines, *Cancer Cell* 40 (2022) 559–564.
- [8] W. Liu, H. Tang, L. Li, X. Wang, Z. Yu, J. Li, Peptide-based therapeutic cancer vaccine: current trends in clinical application, *Cell Prolif.* 54 (2021) e13025.
- [9] L. Bezu, O. Kepp, G. Cerrato, J. Pol, J. Fucikova, R. Spisek, et al., Trial watch: peptide-based vaccines in anticancer therapy, *OncImmunology* 7 (2018) e1511506.
- [10] X. He, S.I. Abrams, J.F. Lovell, Peptide delivery systems for cancer vaccines, *Adv. Ther.* 1 (2019) 1800060.
- [11] M. Kaczmarek, J. Poznańska, F. Fechner, N. Michalska, S. Paszkowska, A. Napierała, et al., Cancer vaccine therapeutics: limitations and effectiveness-A literature review, *Cells* 12 (2023).
- [12] F. Zahedipour, K. Jamialahmadi, P. Zamani, M. Reza Jaafari, Improving the efficacy of peptide vaccines in cancer immunotherapy, *Int. Immunopharm.* 123 (2023) 110721.
- [13] A.N. Tsoras, J.A. Champion, Protein and peptide biomaterials for engineered subunit vaccines and immunotherapeutic applications, *Annu. Rev. Chem. Biomol. Eng.* 10 (2019) 337–359.
- [14] Y. Zhang, H. Xu, L. Jiang, Z. Liu, C. Lian, X. Ding, et al., Sulfonium-driven neoantigen-released DNA nanodevice as a precise vaccine for tumor immunotherapy and prevention, *ACS Nano* 16 (2022) 19509–19522.
- [15] A. Goloś, A. Lutyńska, Aluminium-adjuvanted vaccines—a review of the current state of knowledge, *Przegl. Epidemiol.* 69 (731–4) (2015) 871–874.
- [16] D. Laera, H. HogenEsch, D.T. O'Hagan, Aluminum Adjuvants-‘Back to the future’, *Pharmaceutics* 15 (2023) 1884.

- [17] G. Ott, G.L. Barchfeld, D. Chernoff, R. Radhakrishnan, P. van Hoogevest, G. Van Nest, MF59 Design and Evaluation of a Safe and Potent Adjuvant for Human Vaccines, Springer US, Boston, MA, 1995.
- [18] N. Garçon, D.W. Vaughn, A.M. Didierlaurent, Development and evaluation of AS03, an Adjuvant System containing α -tocopherol and squalene in an oil-in-water emulsion, *Expert Rev. Vaccines* 11 (2012) 349–366.
- [19] H. Kobayashi, A.A. Horner, K. Takabayashi, M.-D. Nguyen, E. Huang, N. Cinman, et al., Immunostimulatory dna prepriming: a novel approach for prolonged Th1-biased immunity, *Cell. Immunol.* 198 (1999) 69–75.
- [20] A. Kaur, J. Baldwin, D. Brar, D.B. Salunke, N. Petrovsky, Toll-like receptor (TLR) agonists as a driving force behind next-generation vaccine adjuvants and cancer therapeutics, *Curr. Opin. Chem. Biol.* 70 (2022) 102172.
- [21] K.A. Martins, S. Bavari, A.M. Salazar, Vaccine adjuvant uses of poly-IC and derivatives, *Expert Rev. Vaccines* 14 (2015) 447–459.
- [22] S.K. Verma, P. Mahajan, N.K. Singh, A. Gupta, R. Aggarwal, R. Rappuoli, et al., New-age vaccine adjuvants, their development, and future perspective, *Front. Immunol.* 14 (2023) 1043109.
- [23] E. Theisen, J.-D. Sauer, *Listeria monocytogenes*-induced cell death inhibits the generation of cell-mediated immunity, *Infect. Immun.* 85 (2017), <https://doi.org/10.1128/iai.00733-16>.
- [24] J.-D. Sauer, S. Pereyre, K.A. Archer, T.P. Burke, B. Hanson, P. Lauer, et al., *Listeria monocytogenes* engineered to activate the Nlr4 inflammasome are severely attenuated and are poor inducers of protective immunity, *Proc. Natl. Acad. Sci. U. S. A.* 108 (2011) 12419–12424.
- [25] R. Deng, H. Zheng, H. Cai, M. Li, Y. Shi, S. Ding, Effects of helicobacter pylori on tumor microenvironment and immunotherapy responses, *Front. Immunol.* 13 (2022).
- [26] S. Kumar Pachathundikandi, S. Brandt, J. Madassery, S. Backert, Induction of TLR-2 and TLR-5 expression by *Helicobacter pylori* switches cagPAI-dependent signalling leading to the secretion of IL-8 and TNF- α , *PLoS One* 6 (2011) e19614.
- [27] N. Pishesha, T.J. Harmand, H.L. Ploegh, A guide to antigen processing and presentation, *Nat. Rev. Immunol.* 22 (2022) 751–764.
- [28] M. Sioud, Releasing the immune system brakes using siRNAs enhances cancer immunotherapy, *Cancers* 11 (2019).
- [29] K. Igarashi, T. Kurosaki, R. Roychoudhuri, BACH transcription factors in innate and adaptive immunity, *Nat. Rev. Immunol.* 17 (2017) 437–450.
- [30] L. Shen, K. Evel-Kabler, R. Strube, S.Y. Chen, Silencing of SOCS1 enhances antigen presentation by dendritic cells and antigen-specific anti-tumor immunity, *Nat. Biotechnol.* 22 (2004) 1546–1553.
- [31] A. Yoshimura, T. Naka, M. Kubo, SOCS proteins, cytokine signalling and immune regulation, *Nat. Rev. Immunol.* 7 (2007) 454–465.
- [32] A. Yoshimura, M. Suzuki, R. Sakaguchi, T. Hanada, H. Yasukawa, SOCS, inflammation, and autoimmunity, *Front. Immunol.* 3 (2012).
- [33] D. Shi, D. Li, Q. Yin, Y. Qiu, H. Yan, Y. Shen, et al., Silenced suppressor of cytokine signaling 1 (SOCS1) enhances the maturation and antifungal immunity of dendritic cells in response to *Candida albicans* in vitro, *Immunol. Res.* 61 (2015) 206–218.
- [34] D. Wang, X.F. Huang, B. Hong, X.-T. Song, L. Hu, M. Jiang, et al., Efficacy of intracellular immune checkpoint-silenced DC vaccine, *JCI Insight* 3 (2018).
- [35] M.Q. Rodrigues, P.M. Alves, A. Roldao, Functionalizing ferritin nanoparticles for vaccine development, *Pharmaceutics* 13 (2021).
- [36] M. Kanekiyo, C.-J. Wei, H.M. Yassine, P.M. McTamney, J.C. Boyington, J.R. Whittle, et al., Self-assembling influenza nanoparticle vaccines elicit broadly neutralizing H1N1 antibodies, *Nature* 499 (2013) 102–106.
- [37] M. Kanekiyo, W. Bu, M.G. Joyce, G. Meng, J.R. Whittle, U. Baxa, et al., Rational design of an Epstein-Barr virus vaccine targeting the receptor-binding site, *Cell* 162 (2015) 1090–1100.
- [38] W. Wang, X. Zhou, Y. Bian, S. Wang, Q. Chai, Z. Guo, et al., Dual-targeting nanoparticle vaccine elicits a therapeutic antibody response against chronic hepatitis B, *Nat. Nanotechnol.* 15 (2020) 406–416.
- [39] L. He, X. Lin, Y. Wang, C. Abraham, C. Sou, T. Ngo, et al., Single-component, self-assembling, protein nanoparticles presenting the receptor binding domain and stabilized spike as SARS-CoV-2 vaccine candidates, *Sci. Adv.* 7 (2021) eabf1591.
- [40] A.E. Powell, K. Zhang, M. Sanyal, S. Tang, P.A. Weidenbacher, S. Li, et al., A single immunization with spike-functionalized ferritin vaccines elicits neutralizing antibody responses against SARS-CoV-2 in mice, *ACS Cent. Sci.* 7 (2021) 183–199.
- [41] L. Mendes-Jorge, D. Ramos, A. Valença, M. López-Luppo, V.M. Pires, J. Catita, et al., L-ferritin binding to scara5: a new iron traffic pathway potentially implicated in retinopathy, *PLoS One* 9 (2014) e106974.
- [42] B. Yu, C. Cheng, Y. Wu, L. Guo, D. Kong, Z. Zhang, et al., Interactions of ferritin with scavenger receptor class A members, *J. Biol. Chem.* 295 (2020) 15727–15741.
- [43] Y. Qu, B. Zhang, Y. Wang, S. Yin, J.L. Pederick, J.B. Bruning, et al., Immunogenicity study of engineered ferritins with C- and N-terminus insertion of Epstein-Barr nuclear antigen 1 epitope, *Vaccine* 39 (2021) 4830–4841.
- [44] T.B. Wyman, F. Nicol, O. Zelpathi, P.V. Scaria, C. Plank, F.C. Szoka Jr., Design, synthesis, and characterization of a cationic peptide that binds to nucleic acids and permeabilizes bilayers, *Biochemistry* 36 (1997) 3008–3017.
- [45] N. Miura, K. Tange, Y. Nakai, H. Yoshioka, H. Harashima, H. Akita, Identification and evaluation of the minimum unit of a KALA peptide required for gene delivery and immune activation, *J. Pharmaceut. Sci.* 106 (2017) 3113–3119.
- [46] M.F. Bachmann, G.T. Jennings, Vaccine delivery: a matter of size, geometry, kinetics and molecular patterns, *Nat. Rev. Immunol.* 10 (2010) 787–796.
- [47] S. Pechmann, E.D. Levy, G.G. Tartaglia, M. Vendruscolo, Physicochemical principles that regulate the competition between functional and dysfunctional association of proteins, *Proc. Natl. Acad. Sci. U. S. A.* 106 (2009) 10159–10164.
- [48] F. Hämmerling, M.M. Pieler, R. Hennig, A. Serve, E. Rapp, M.W. Wolff, et al., Influence of the production system on the surface properties of influenza A virus particles, *Eng. Life Sci.* 17 (2017) 1071–1077.
- [49] E.M. Cheng, N.W. Tsarovsky, P.M. Sondel, A.L. Rakhmievich, Interleukin-12 as an in situ cancer vaccine component: a review, *Cancer Immunol. Immunother.* 71 (2022) 2057–2065.
- [50] M. Kurachi, CD8+ T cell exhaustion, *Semin. Immunopathol.* 41 (2019) 327–337.
- [51] H. Jiang, Q. Wang, L. Li, Q. Zeng, H. Li, T. Gong, et al., Turning the old adjuvant from gel to nanoparticles to amplify CD8+ T cell responses, *Adv. Sci.* 5 (2018) 1700426.
- [52] D. Martínez-Pérez, D. Viñal, I. Solares, E. Espinosa, J. Feliu, Gp-100 as a novel therapeutic target in uveal melanoma, *Cancers* 13 (2021) 5968.
- [53] D. Minor, gp100 peptide vaccine in melanoma, *N. Engl. J. Med.* 365 (2011) 771.
- [54] T.N. Schumacher, R.D. Schreiber, Neoantigens in cancer immunotherapy, *Science* 348 (2015) 69–74.
- [55] J. Guo, L. Tang, K. Li, Q. Ma, S. Luo, R. Cheng, et al., Application of nanotechnology in therapeutic cancer vaccines, *Adv NanoBiomed Res* 3 (2023) 2200122.
- [56] M.J. Lin, J. Svensson-Arvelund, G.S. Lubitz, A. Marabelle, I. Melero, B.D. Brown, et al., Cancer vaccines: the next immunotherapy frontier, *Nat. Can. (Ott.)* 3 (2022) 911–926.
- [57] U. Sahin, Ö. Türeci, Personalized vaccines for cancer immunotherapy, *Science* 359 (2018) 1355–1360.
- [58] M. Cully, Personalized cancer vaccines hit the spot, *Nat. Rev. Drug Discov.* 17 (2018) 393.
- [59] S. Kageyama, Y. Nagata, T. Ishikawa, T. Abe, M. Murakami, T. Kojima, et al., 1214P - randomized phase II clinical trial of NY-ESO-1 protein vaccine combined with cholesterol pullulan (CHP-NY-ESO-1) in resected esophageal cancer patients, *Ann. Oncol.* 30 (2019) v496.
- [60] M.E. Janes, A.P. Gottlieb, K.S. Park, Z. Zhao, S. Mitragotri, Cancer vaccines in the clinic, *Bioeng Transl Med* 9 (2024) e10588.
- [61] B. Wolfson, S.E. Franks, J.W. Hodge, Stay on target: reengaging cancer vaccines in combination immunotherapy, *Vaccines* 9 (2021) 509.
- [62] C. Schmidt, Personalized cancer vaccines advance in the clinic, *J. Natl. Cancer Inst.* 109 (2017).
- [63] Y. Ding, Z. Li, A. Jaklenc, Q. Hu, Vaccine delivery systems toward lymph nodes, *Adv. Drug Deliv. Rev.* 179 (2021) 113914.
- [64] L. Wei, C. Dong, W. Zhu, B.-Z. Wang, mRNA vaccine nanoplatfoms and innate immunity, *Viruses* 16 (2024) 120.
- [65] C. Gouttefangeas, H.-G. Rammensee, Personalized cancer vaccines: adjuvants are important, too, *Cancer Immunol. Immunother.* 67 (2018) 1911–1918.
- [66] J.P. Snook, C. Kim, M.A. Williams, TCR signal strength controls the differentiation of CD4+ effector and memory T cells, *Sci Immunol* 3 (2018) eaas9103.
- [67] S. Solouki, W. Huang, J. Elmore, C. Limper, F. Huang, A. August, TCR signal strength and antigen affinity regulate CD8+ memory T cells, *J. Immunol.* 205 (2020) 1217–1227.
- [68] P. Juanes-Velasco, A. Landeira-Viñuela, V. Acebes-Fernandez, Á.-P. Hernández, M. L. Garcia-Vaquero, C. Arias-Hidalgo, et al., Deciphering human leukocyte antigen susceptibility maps from immunopeptidomics characterization in oncology and infections, *Front. Cell. Infect. Microbiol.* 11 (2021).
- [69] D. García-Azorín, T.P. Do, A.R. Gantenbein, J.M. Hansen, M.N.P. Souza, M. Obermann, et al., Delayed headache after COVID-19 vaccination: a red flag for vaccine induced cerebral venous thrombosis, *J. Headache Pain* 22 (2021) 108.
- [70] X. Pang, H. Liu, X. He, T. Ji, Y. Zhu, Y. Cui, Potential anionic substances binding to platelet factor 4 in vaccine-induced thrombotic thrombocytopenia of ChAdOx1-S vaccine for SARS-CoV-2, *Front. Immunol.* 12 (2022).
- [71] M.G. Joyce, W.-H. Chen, R.S. Sankhala, A. Hajduczek, P.V. Thomas, M. Choe, et al., SARS-CoV-2 ferritin nanoparticle vaccines elicit broad SARS coronavirus immunogenicity, *Cell Rep.* 37 (2021).
- [72] M.G. Joyce, H.A.D. King, I. Elakhal-Naouar, A. Ahmed, K.K. Peachman, C. Macedo Cincotta, et al., A SARS-CoV-2 ferritin nanoparticle vaccine elicits protective immune responses in nonhuman primates, *Sci. Transl. Med.* 14 (2022) eabi5735.
- [73] B.L. Ober Shepherd, P.T. Scott, J.N. Hutter, C. Lee, M.D. McCauley, I. Guzman, et al., SARS-CoV-2 recombinant spike ferritin nanoparticle vaccine adjuvanted with Army Liposome Formulation containing monophosphoryl lipid A and QS-21: a phase 1, randomised, double-blind, placebo-controlled, first-in-human clinical trial, *The Lancet Microbe* 5 (2024) e581–e593.
- [74] J.A. Miranda, K. Fenner, P.B. McKinzie, V.N. Dobrovolsky, J.R. Revollo, Unbiased whole genome detection of ultrarare off-target mutations in genome-edited cell populations by HiFi sequencing, *Environ. Mol. Mutagen.* 64 (2023) 374–381.